THE TRANSPORT OF PLASTIC DEBRIS IN COASTAL SEAS: RESULTS OF PHYSICAL MODELING

Faraci C.[1], Bonanno G.[1], Passalacqua G.[1], Cucinotta F.[1], Iuppa C.[1]

The nearshore zone turns out to be the area with the highest concentration of plastic debris and, for this reason, it is important to know the processes that affect the motion and the fate of this type of litter. Two experimental campaigns were conducted: the first one analyses the transport on a horizontal bottom, while the second one focuses on studying the upwelling of micro- and macroplastic particles on an inclined plane with a variable slope. Both fixed bottoms (smooth and rough) and a mobile bed were considered. The main aim is to characterise the transport under wave action for different boundary conditions in order to get a complete picture of the hydrodynamic process that is taking place with the wave propagation from offshore towards the beach.

Keywords: plastic pollution; Blob Analysis; transport; sloping bed.

INTRODUCTION

Plastic pollution has became a widespread phenomenon with significant implications for ecosystems and organisms in a variety of forms (Ivar do Sul and Costa, 2014). It is estimated that plastic production will reach 500 million tons in 2025 (Du et al., 2021). The trajectory and speed of plastics are controlled by their physical characteristics (density, size, and shape) and ocean dynamic conditions (wind, waves, tides, thermohaline gradients, and the influence of benthic sediments) (Zhang, 2017). Moreover, plastics can be buoyant or non-buoyant.

Microplastics, defined as plastic particles smaller than 5 mm, originate either from the degradation of larger plastic objects (secondary microplastics) or from direct sources (primary microplastics). This work will focus specifically on non-buoyant plastics, in which the transport process is dependent on the bed roughness which may alter the wave-current interaction along the column (Faraci et al., 2021). In particular, a particle will only mobilize when the combined force of drift and lift exceeds the gravitational force acting upon it. These forces are further influenced by various physical and mechanical properties such as density and shape.

A conceptual basis to understand and predict plastic behaviour in nearshore areas is through sediment transport (Forsberg et al. (2020)). While research on sediment transport is well-established (Madsen and Grant (1976), Nielsen (1988), Van Rijn (2007), Shields (1936), Manohar and Board (1955), Bagnold and Taylor (1946)), the dynamics of microplastic transport remain not so much explored in the current literature. Some recent experimental studies on incipient motion or sedimentation of plastic particles (Goral et al. (2023), Francalanci et al. (2021), Komar and Miller (1975), Waldschlager and Schuuttrumpf (2019), Guler et al. (2022)) are all referred to steady flow condition.

In fact, the mechanisms that affect plastic movement in marine environments is non thoroughly explored. This study is aimed to fill this gap, and seeks to characterize the transport processes of non-buoyant plastics with varying shapes and densities on a large scale. It involves a beach profile with a variable slope as well as a horizontal bottom to analyze solid transport under differing seabed conditions.

The research examines various bed sediment grain sizes and transport dynamics on both sloping and horizontal planes within specific scenarios: i) a fixed and smooth seabed, ii) a fixed and rough seabed, iii) a mobile horizontal seabed with a median grain size D_{50} of 0.21 mm. By investigating these scenarios, the study provides valuable insights into plastics and microplastic (MP) transport across varying hydrodynamic and seabed conditions, thereby enhancing our understanding of their behavior in marine systems.

METHODOLOGY

Experiments were carried out at the Hydraulic Laboratory of the University of Messina inside an 18.5 m long wave channel and a rectangular cross-section of 0.4 m x 0.8 m. The characteristics of the samples used during the two campaigns are set out below.

Only regular waves were generated. Samples were placed in different ways in function of the setup conditions (Fig.1.a and Fig. 1.b) , constantly recorded by a cameras with a resolution of 1920 x 1080 pixels, 30 x zoom (4 K), 28.8 mm wide angle lens, and a frame rate of 50 fps. The channel was equipped with three

[1]University of Messina, Italy

resistive gauges to measure wave elevation and a Vectrino Profiler, set at four different depths to measure the velocity of the fluid and trace its vertical profile.

Two different bottom configurations were considered. The first is a horizontal bed (T-1), realized with a layer of sand with d_{50} of 0.21 mm. In the presence of strong waves, due to the formation of ripples, however, it was replaced with a rough fixed bottom with the same grain size (T-2). The second is a fixed sloping bed, with different bed roughess, smooth (S-1) or rough (S-2).

Table 1: Sample properties: id particle, shape, the long side a, short side b, thickness c, the Corey Shape Factor CSF and the sample density ρ_ρ

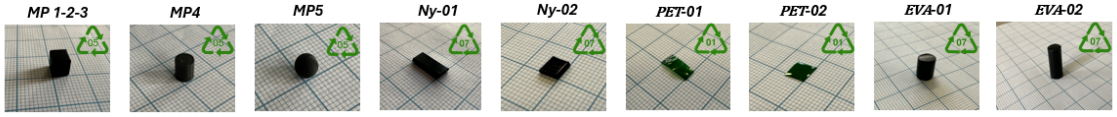

Id	Shape	Material	a $[cm]$	b $[cm]$	c $[cm]$	CSF	ρ_p $[g/cm^3]$	w_s^2 $[m/s]$	C_d
MP1	Cube	PLA	0.5	0.5	0.5	1.000	1.26	0.1424	1.26
MP2	Cube	PLA	0.5	0.5	0.5	1.000	1.10	0.1137	0.8
MP3	Cube	PLA	0.5	0.5	0.5	1.000	1.03	0.0713	0.66
MP4	Cylinder	PLA	0.5	0.5	0.5	1.000	1.26	0.1466	0.93
MP5	Sphere	PLA	0.5	0.5	0.5	1.000	1.25	0.1548	0.69
Ny-01	Plate	Nylon	1.05	0.5	0.08	0.110	1.14	0.0461	1.31
Ny-02	Plate	Nylon	0.5	0.5	0.08	0.159	1.14	0.0517	1.05
PET-01	Plate	PET	1.05	0.5	0.011	0.015	1.37	0.0314	1.07
PET-02	Plate	PET	0.6	0.6	0.011	0.018	1.37	0.0339	1.01
EVA-01	Cylinder	EVA	0.7	0.6	0.6	0.926	1.02	0.0403	0.74
EVA-02	Cylinder	EVA	1.45	0.6	0.6	0.643	1.02	0.0437	0.75

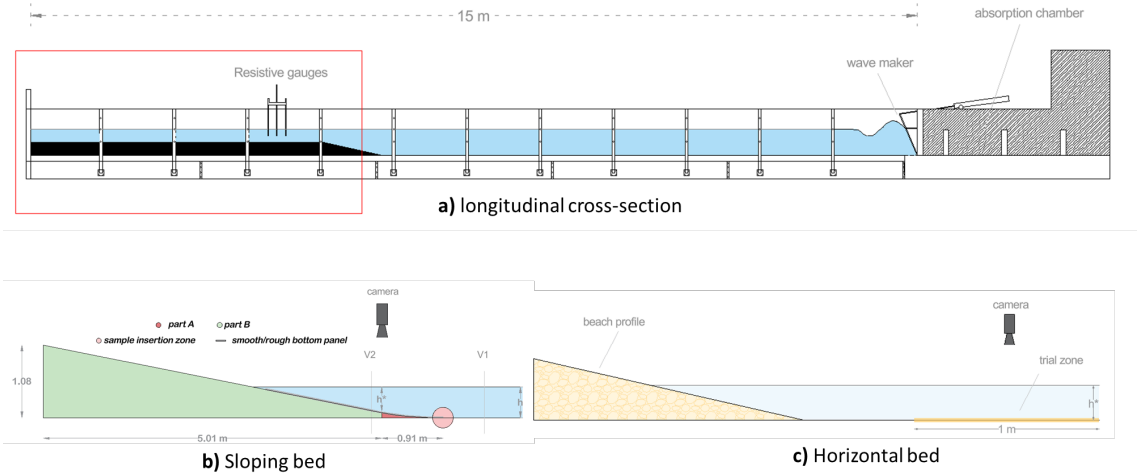

Figure 1: longitudinal cross-section of the wave flume used in the experimental campaign used for sloping (a) and horizontal (b) transport. The symbol V indicates the positions of the Vectrino Profiler (Nortek As.). The initial slope of the submerged beach (part A) was designed to have a gradually varying slope. The part B is characterised by a constant slope equal to 20 %. The thick grey line on the slope indicates the area with controlled roughness.

Eleven samples were tested, as reported in Tab.1. Three cubes (MP1, MP2, MP3), a sphere (MP4) and a cylinder (MP5), with same dimensions but different density, were 3D printed; two Nylon cable ties (Ny-01,Ny-02) two PET fragments (PET-1,PET-2) and two EVA cylinders (EVA-01, EVA-02) which were

Table 2: Simulated hydrodynamic conditions for the transport on an horizontal mobile (T-1) and fixed bottom (T-2): water depth offshore (h), water depth near the trial zone ($h*$), wave period (T), wave length (L), and incident wave height range (H).

bottom type	h [m]	$h*$ [m]	T [s]	L [m]	H [m]
T-1	0.4	0.15	1.66	1.93	0.003 - 0.073
	0.37	0.15	1.66	1.74	0.047 - 0.083
T-2	0.37	0.15	1.25	1.27	0.070 - 0.087
	0.37	0.15	1.00	0.99	0.075 - 0.087

Table 3: Simulated hydrodynamic conditions for transport on sloping smooth fixed bottom (S-1) and rough fixed bottom (S-2): water depth at the initial point (h), wave period (T), wave length (L), and incident wave height range (H)., reflection (k_r) and the Irribarren number (ϵ)

bottom type	h [m]	T [s]	L [m]	H [m]	k_r	ϵ
	0.23	1.00-1.66	1.273-2.355	0.015-0.064	0.15-0.57	0.63-2.52
S-1, S-2	0.18	1.00-1.66	1.172-2.109	0.018-0.098	0.18-0.59	0.69-2.14
	0.15	1.00-1.66	1.094-1.956	0.021-0.084	0.15-0.46	0.72-1.95

instead modeled or cut from their primary form. For each sample three dimensions, a, b and c were defined, referring respectively to the long side, short side and thickness of the individual elements. The thickness c ranges from values of 0.1 mm to 8 mm and presents the highest variability among the plastic characteristics. A characteristic parameter of particle shape is the Corey Shape Factor $CSF = c/\sqrt{ab}$. Density ρ_ρ was measured with a hydrostatic precision balance. C_d is the drag coefficient valued as $\frac{2g(s-1)V}{w_s^2 A}$

In experiments with horizontal configuration (T1, 2), EVA particles were not considered, while for sloping configuration (S1, 2) only Ny, PET and EVA samples were considered. Between one test and the successive, the channel was left in still conditions in order to start all the tests from rest. The scaling approach used in the present work considers the sand model (Hughes (1994)) renouncing to scale the sediments and plastics. The simulated hydrodynamic conditions are synthesized in Tab. 2 and Tab. 3. .

Experimental setup and methodology in the horizontal bottom

As reported in Fig. 1.a, in red the trial zone of the flume is framed where a sand layer (T-1) characterized by a diameter of d_{50} = 0.21 mm for a thickness of about 3 cm was set for the first experimental campaign. To ensure consistent conditions for comparison, the moving sand bottom was replaced with a fixed bottom, with a rough surface obtained by gluing the same sand (T-2) over an aluminum panel. This setup adjustment was necessary because, propagating very steep waves, not only the mobilization of plastic particles but also the mobilization of sediments was observed. A fixed bottom helped to prevent the formation of bottom sedimentary structures that could disturb or alter the dynamics of the plastic particles. Additionally, two fixed steel bars, equipped with 10 red bolts each , were positioned on either side of the investigation zone. Continuous monitoring, including the estimation of the particle group position over time, was performed using video analysis recorded with the aforementioned camera, employing the Blob Analysis technique.

Blob Analysis is a method for detecting homogeneous regions of pixels (blobs) in an image that differ in features and properties from surrounding pixels (Moeslund, 2012). The evolution of the particle group over time was monitored continuously by the video camera placed above the trial zone, and the videos were analyzed using the methodology described in Fig. 2. For each frame (frame rate=50 per second), the position of the global centroid of the particle group, i.e., its center of mass ($X_{g,s}$), was identified. Since the particle group is subjected to an oscillating force, the signal of the displacement of its centroid ($X_{g,s}$) can be split into two components: a drift component (in red in Fig. 3) and an oscillating component (in green in Fig. 3). In this analysis, the complete signal was examined, which includes both the oscillating and drift components. This combination allows for a more comprehensive assessment of particle dynamics, which can change based on variations in particle characteristics and external forces. Velocity was estimated as the average of the velocities for each wave cycle in tests when continuous video analysis was performed. In few cases velocity was calculated as the difference in the centroid position between the final and initial

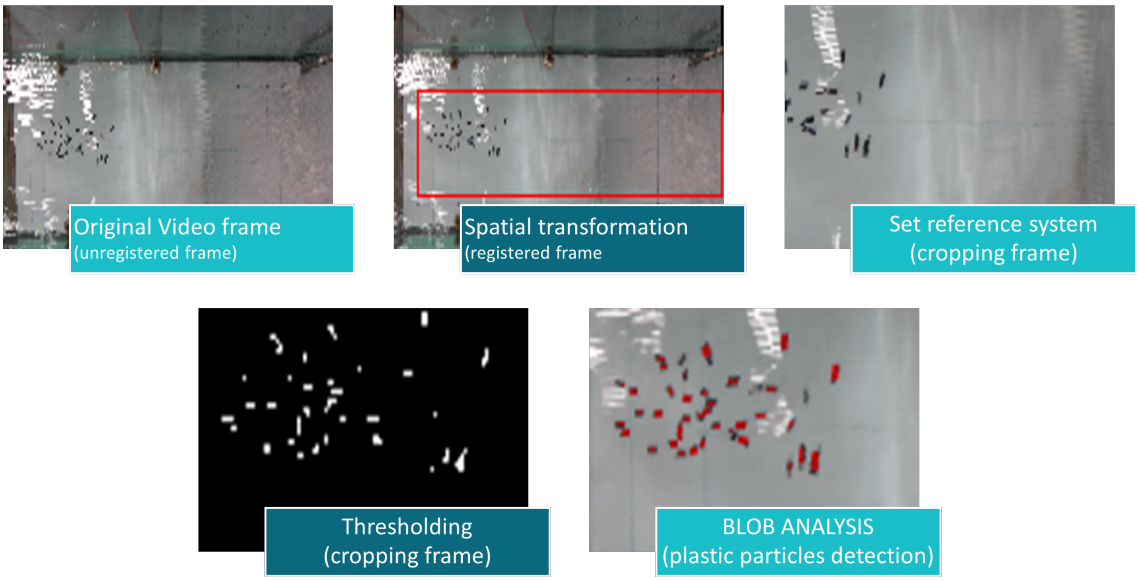

Figure 2: The main steps performed on each video are as follows: i) dividing the video into frames; ii) spatially transforming the frames; iii) converting the frames from RGB to binary images; iv) applying blob analysis; and v) filtering the signal to eliminate noise.

frames, divided by the elapsed time.

This methodology enabled the analysis of each video frame and, after conducting a few preliminary operations, the identification of each plastic particle and the localization of the global centroid whose displacement was tracked over time. The preliminary operations included spatial transformation and orthonormalization to minimize perspective distortions in the images; the application of a filter on the RGB color space (as shown in Fig. 2); and the use of a low-pass filter with a cutoff frequency set at two times the frequency of the incident wave, to mitigate image deformation caused by the wave crest passing over the water surface. The adopted methodology was calibrated and validated in previous studies (Passalacqua et al., 2023).

Experimental setup and methodology in the sloping bottom case

In this case, a sloping bed (see Fig. 1.b) was inserted at the end of the channel. The slope has a curved part (part A, in red) and a constant slope of 20% (part B, in green). Three different depths were considered. Each run lasted up to 120 s, the time needed to mobilize the samples and reach their ultimate position.

Each sample, consisting of 100 particles, was placed at the beach toe at the beginning of each test. The tracking of the plastic particles, moved by wave action, was conducted through post-processing analysis of images captured by a video camera. The camera was positioned allowing for overhead monitoring of the sample evolution over time and enabling the tracking of particle movements using blob analysis. The main steps performed on each video are as follows: i) dividing the video into frames; ii) spatially transforming the frames; iii) converting the frames from RGB to binary images; iv) applying blob analysis; and v) filtering the signal to eliminate noise. For each frame, the coordinates of the global centroid, i.e. the centre of masses of the whole sample, were estimated (Xg,s). For further details about the frame analysis and the method to estimate Xg, s please refer to (Passalacqua et al. (2023)). At the equilibrium point, when the drift component Xg assumes a constant value, the maximum values of the drift component, depth, and slope are denoted respectively by the symbols $X_{g,max}$, $h_{g,max}$, and $\alpha_{g,max}$, respectively.

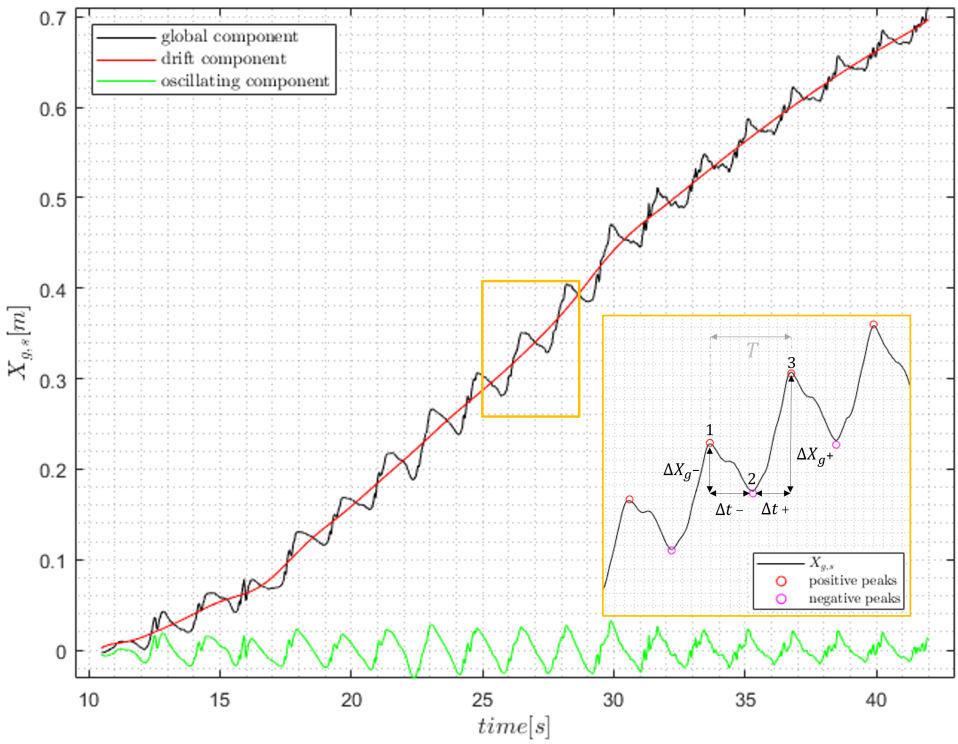

Figure 3: Variation over time of the centroid of a group of plastic particles: global component (in black), drift component (in red) and oscillating component (in green). The test was carried out for sample MP1 with the following hydrodynamic conditions: h=0.15 m, T=1.66 s, L=1.93 m and H=0.7 m.

RESULTS

In this section, the transport process will be analysed. In particular, the transport on the horizontal bed will focus on the particle velocity and how the shape can influence the transport under wave motion. A corrective factor is prpoposed in order to establish a correspondence between the hydrodynamic conditions and geometrical particle properties. In the sloping bed case, the focus will be on the propensity of the particles to drift in the presence of different conditions such as bed roughness, water depht h, wave height H, wave period T.

Transport on an horizontal mobile and fixed bottom

This section discusses results on continuous tracking of groups of non-buoyant MP particles moving on a sandy flat bottom under regular wave action. The analysis of various plastic samples and different hydrodynamic conditions allowed the group dynamics to be studied and some characteristic values, such as velocity to be extracted. In particular, it was observed that the transport of the different samples is closely related to their geometric and physical properties.

The analysis on the transport of plastic samples was carried out, as already described, by tracking the position of its centroid $X_{g,s}$ over time. The samples show different transport propensities due to their different shape and density characteristics and to the simulated hydrodynamic conditions. As previously discussed, particle dynamics is significantly influenced by the oscillatory component. We estimated a characteristic parameter for each sample depending on variations in wave conditions. This parameter, defined as dynamic oscillation factor Of reflects the propensity for oscillation, defined as the difference between forward velocity (during positive phase) and backward velocity (during negative phase).

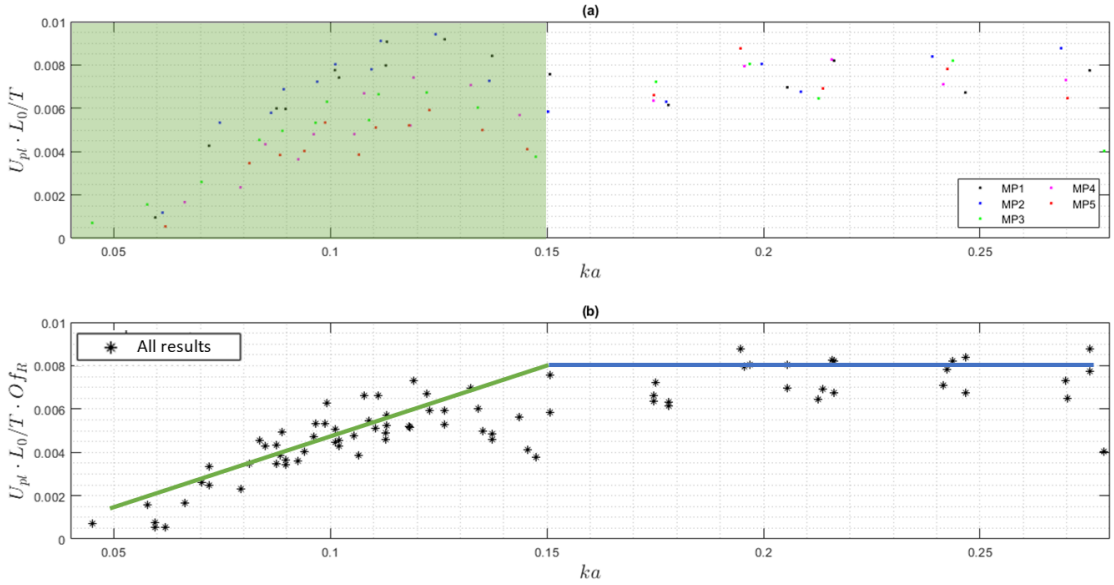

Figure 4: (a) Non dimensional plastic velocity as a function of the wave steepness ka; (b) Non dimensional plastic velocity as a function of the wave steepness ka and the relative oscillation coefficient Of_R. The asterisks represent the results of all samples and the curve the interpolation with a 1st degree polynomial.

The dynamic oscillation factor (Of) was calculated as follows:

$$Of = \frac{v^+}{v^-} \tag{1}$$

Where v^+ and v^- are respectively the positive and negative phase velocities of each wave cycle (see Fig. 3) calculated as:

$$v^+ = \frac{\Delta X^+_{g,s}}{\Delta t^+} \qquad v^- = \frac{\Delta X^-_{g,s}}{\Delta t^-} \tag{2}$$

Where $\Delta X^+_{g,s}$ and $\Delta X^-_{g,s}$ are the coordinate differences of the global centroid $X_{g,s}$ between the i-th positive peak and the successive negative peak and between the i-th negative peak and the successive positive peak, and Δt^- and Δt^+ are the corresponding time differences.

In order to characterize the bed transport of the plastic sample group under different hydrodynamic conditions, the value of the mean global centroid velocity (U_{pl}) was divided by the wave celerity (L_0/T) and plotted as function of the wave steepness (ka) in Fig.4.a. It is notable that samples MP1 (cube with density ρ_p=1.26 g/cm^3) and MP2 (cube with density ρ_p=1.10 g/cm^3) exhibit dynamic oscillation factors Of values that depend on wave motion, increasing with the wave steepness ka. This trend indicates that the oscillation velocity during the positive phase becomes increasingly greater than that during the negative phase as ka increases. Sample MP3, a cube with a density of $\rho_p = 1.03 g/cm^3$ exhibits a slight increase in Of with higher ka values; however, this effect is minimal. On the contrary, samples MP4, cylinders with a density of $\rho_p = 1.26 g/cm^3$, and MP5, i.e. spheres with a density of $\rho_p = 1.25 g/cm^3$, show a nearly constant dynamic oscillation factor that remains unaffected by variations in wave conditions. In order to consider such combined effect of shape and density, a corrective coefficient was introduced in order to normalize the data and obtain comparable results as in Fig.4.b . This coefficient, defined *relative oscillation factor* Of_R (eq. 3), is calculated as the ratio of the oscillation factor of the sphere (Of_{sphere}) and that of the considered plastic (Of_{i-pl}):

$$f(x) = \begin{cases} Of_R = \frac{Of_{sphere}}{Of_{i-pls}} & \text{for} \quad ka < 0.15 \\ Of_R = 1 & \text{for} \quad ka < 0.15 \end{cases} \tag{3}$$

As shown in Fig. 4*b*, it can be seen that the application of the relative oscillation factor greatly reduces the dispersion of the results. The 1st degree polynomial, obtained for values of $ka < 0.15$ has an equation of the type:

$$U_{pL}\frac{L_0}{T}Of_R = 0.013ka + 0.0043 \qquad \text{for} \quad ka < 0.15 \quad R^2 = 0.60 \tag{4}$$

$$U_{pL}\frac{L_0 Of_R}{T} = 0.008 \qquad \text{for} \quad ka > 0.15 \qquad R^2 = 0.60 \tag{5}$$

Transport on sloping fixed bottom

In general, as mentioned before, the transport process is influenced by the shape and the density of plastic samples but also by the different bottom grain size. An example of three types of motion detected during the experimental campaign is shown in Fig. 5. To compare the dynamic of the various plastic samples, the slope was divided into five equal parts. Point b is the transition between A and B zones (see Fig. 1 a). Point d is the point in which the samples start to be surely affected by the wave breaking. Points a and c are respectively the midpoints of the curved ramp and of section b-d. The average slope angle is approximately equal to 2° and 7.82 ° for Zone 1 and Zone 2 respectively. Zones 3-4-5 are characterised by a constant slope angle equal to 11.31° .

For each test, the weighted centroid is is constantly estimated in order to know its position.

$$X'_g = \frac{\sum_{i=1}^{n_z} X_{g,i}t_i}{\sum_{i=1}^{n_z} t_i} \tag{6}$$

where n_z is the number of zones, ti is the residence time of the centroid within i-th zone and $X_{g,i}$ is the average position of the centroid in the i-th zone.

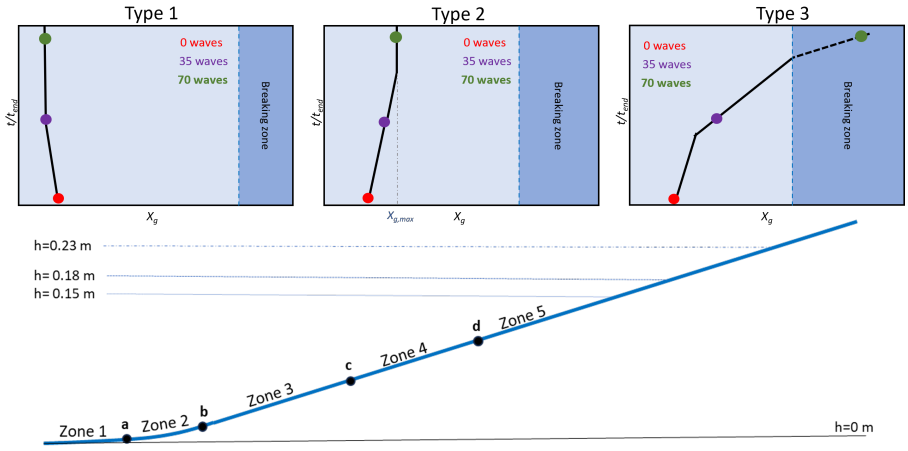

Figure 5: Three examples of plastic debris transport due to waves. First column: type 1; second column: type 2; third column: type 3.

In Fig. 5 the point on the frame indicates the position of the centroid in three different times corresponding to the passage of 0 waves, 35 waves and 70 waves, which mimics the centroid displacement during the test. Three types of motion can be identified: net zero transport (type 1), transport to an equilibrium point (type 2) and transport to the breaking zone (type 3). The corresponding hydrodynamic conditions are: H=1.5 cm, T=1.67 s and h=23 cm (type 1); H=4.4 cm, T=1.25 s and h=18 cm (type 2); (type 3) H=8.4 cm, T=1.00 s and h=18 cm.

Table 4: $\Delta P_{p,size}$ and $\Delta P_{p,bed}$ estimated for the samples. Negative value of $\Delta P_{p,size}$ indicates more resistance of the larger size particles than the smaller size particles. Negative value of $\Delta P_{p,bed}$ indicates more resistance of the particles on the smooth bed than rough bed. Values close to zero indicate similar behaviour between the compared configurations.

Material	$\Delta P_{p,bed}$		$\Delta P_{p,bed}$	
	smooth bed	rough bed	larger size	smaller size
PET	21.13	12.54	-14.36	-24.72
NY	-77.18	-5.49	-81.33	-7.31
EVA	-44.14	-1.50	10.95	34.01

By normalising X_g' according to the wave parameters, it is possible to extrapolate the particle drift capacity. In particular, a linear law was assumed for each sample and a fixed water depth:

$$\frac{X_g'}{L_0} = P_p k_0 a \tag{7}$$

in which L_0 is the wave length, k_0 wave number in deep water and a wave amplitude. Therefore, if P_p is the measure of the propensity of the particles to be drifted, high P_p values indicates low resistance of the particles to motion and vice versa. The comparison between the various P_p values was quantified through two parameters: $\Delta P_{p,size}$ and $\Delta P_{p,bed}$ which are respectively two coefficient useful for the comparison between different particles in terms of dimensions and bottom bed.

$$\Delta P_{p,size} = \frac{\overline{P}_{p,sample,1} - \overline{P}_{p,sample,2}}{\overline{P}_{p,sample,1}} 100 \tag{8}$$

$$\Delta P_{p,bed} = \frac{\overline{P}_{p,sample,1,smooth} - \overline{P}_{p,sample,1,rough}}{\overline{P}_{p,sample,1,smooth}} \tag{9}$$

where $\overline{P}_p$ is the averaged value of P_p for different water depths.

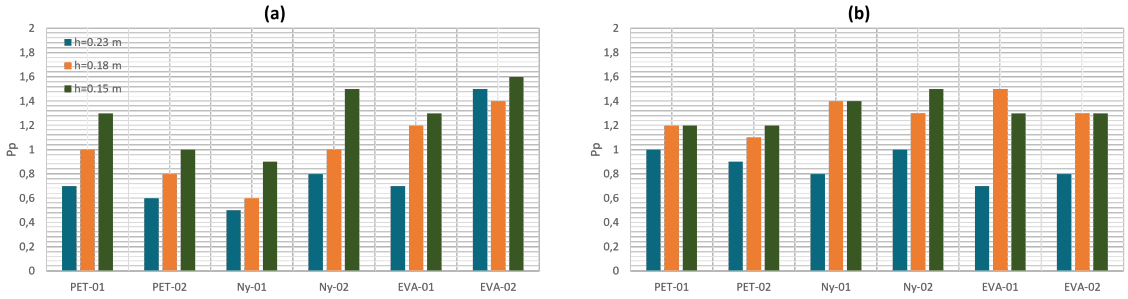

Figure 6: Pp provides a measure of the propensity of the particles to drift on the smooth surface (a) and rough surface (b): high values indicate low resistance of the particles to motion to the current generated by waves.

In general, it can be observed that the reduction in particle displacement occurs due to: i) a decrease in wave steepness; ii) an increase in depth; iii) an increase in particle size; iv) an increase in plastic density. (Iuppa et al. (2024)). In general, there is a greater propensity for smaller water depth and a smooth surface. Samples EVA-01 and EVA-02 exhibit transport dynamics significantly influenced by their low density, causing the elements to jump and fluctuate, which reduces their contact with the bed. It was observed that contact with the surface primarily occurs during the positive oscillation phase, while it is diminished in the negative phase due to the bouncing of the elements. This means that the effect of the roughness only influences the advancement phase and there is no friction effect in the phase opposite to the wave propagation direction. An increase in particle resistance to fluctuations results in enhanced transport on

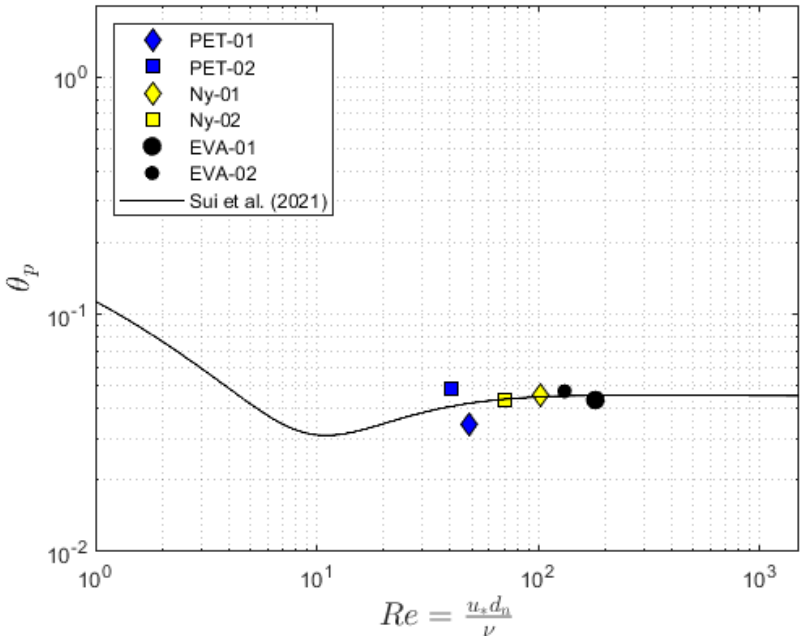

Figure 7: $\theta_p = \theta/\gamma_s$ as a function of the ratio $u * Dn/\nu$. The graph shows the approximated Shields curve proposed by Sui et al. (2021). The coloured data points represent the mean value of all conditions classified as Type 2 for each plastic.

a rough surface. Therefore, it is possible to correlate a geometric condition, such as position X_g, with a mechanical characteristic of the particles, specifically the drag coefficient C_d. More in detail:

$$\gamma_f = \frac{\overline{X}_{g,smooth}}{\overline{X}_{g,rough}} = -1.25C_d + 2.32 \tag{10}$$

Identifying the type of motion is essential for forecasting short-term fate models of plastic. Once equilibrium is reached, $\Delta X_g/\Delta t$ equals 0 in motion Type 2. In order to consder an average equilibrium condition for the tested samples, in Fig. 7, a relationship can be established between stabilizing and destabilizing forces using Shields (1936) threshold parameter θ

$$\theta = \frac{u_*^2}{g(s-1)D_n} \tag{11}$$

which can be generalized for sloping case:

$$\theta_p = \frac{u_*^2}{\gamma_s g(s-1)D_n(1 + tan(\alpha_{g,max}))} \tag{12}$$

where $\alpha_{g,max}$ is the bed slope, D_n is the nominal diameter of the volume-equivalent sphere (Tab. 1 and u_* is the friction velocity estimated according to Jonsson (1967).

The equilibrium condition requires that the force displacing particles offshore must counterbalance the displacement achieved during the positive phases of the waves. In this campaign, it was observed that for the plastic samples to reach these conditions, a value of θ_p is needed that deviates from the Shields curve (θ) by an amount γ_s that depends on the plastic density. It has been observed that γ_s follows a two grades equation:

$$\gamma_s = 65.17s^2 - 165.08s + 104.52 \tag{13}$$

CONCLUSION

This study analyzed the dynamics of non-buoyant plastic samples under sea waves, identifying various types of motion and the effects related to hydrodynamic conditions, plastic properties, and bed characteristics. On horizontal bed, it was found that since the particle group is subjected to an oscillating force,

the signal of the displacement of its centroid ($X_{g,s}$) can be split into two components: a drift component and a oscillating component. This differentiation is important because the oscillating component is affected not only by the wave properties but also by the geometrical plastic properties. An oscillation factor O_f representing the ratio of the positive to the negative phase velocities of each wave cycle. It has been found to be crucial for predicting the transport velocity of each particle, irrespective of the boundary conditions. This coefficient does not seem to be significantly affected by steepness values greater than 0.15, likely because, at very high wave heights, the drift component becomes much more prominent than the oscillating component.

In the sloping bed case, it was found that as wave steepness increases, the displacement of plastic samples from their initial position also increases. The distance traveled by the particles is influenced by the characteristics of the bed, as well as the shape and density of the plastics. On rough surfaces, the differences among the various plastics tend to diminish. The bed roughness leads to non-linear behavior, primarily determined by the particles' resistance to fluctuations. Greater displacement was observed on rough surfaces for plastics with high resistance to vertical movement, while those with low resistance traveled further on smooth surfaces. For a fixed density, larger volume particles generally cover shorter distances; however, an opposite trend was noted for PET. The analysis of tests conducted under equilibrium conditions allowed for the identification of a criterion to distinguish the types of movement that mobilize plastic. By applying commonly used approaches to determine incipient sediment motion conditions, average equilibrium states are established when the threshold parameter θ_p values approach the Shields curve.

ACKNOWLEDGEMENTS

This research has been financially supported by the Italian MUR projects PRINPNRR2022 P2022S2WJZ PLAstic Transport due to waves and currents ON Emerged and submerged beaches (PLATONE) CUP J53D23002680006 - PRIN_2022BCJ5W3_001

References

R. A. Bagnold and G. Taylor. Motion of Waves in Shallow Water. Interaction between Waves and Sand Bottoms. *Proceedings of the Royal Society of London Series A*, 187(1008):1–18, Oct. 1946. doi: 10.1098/rspa.1946.0062.

H. Du, Y. Xie, and J. Wang. Microplastic degradation methods and corresponding degradation mechanism: Research status and future perspectives. *Journal of Hazardous Materials*, 418:126377, 2021. ISSN 0304-3894. doi: https://doi.org/10.1016/j.jhazmat.2021.126377. URL https://www.sciencedirect.com/science/article/pii/S0304389421013418.

C. Faraci, R. E. Musumeci, M. Marino, A. Ruggeri, L. Carlo, B. Jensen, E. Foti, G. Barbaro, and B. ElsaÃŸer. Wave- and current-dominated combined orthogonal flows over fixed rough beds. *Continental Shelf Research*, 220:104403, 2021. ISSN 0278-4343. doi: https://doi.org/10.1016/j.csr.2021.104403. URL https://www.sciencedirect.com/science/article/pii/S0278434321000601.

P. L. Forsberg, D. Sous, A. Stocchino, and R. Chemin. Behaviour of plastic litter in nearshore waters: First insights from wind and wave laboratory experiments. *Marine pollution bulletin*, 153:111023, 2020.

S. Francalanci, E. Paris, and L. Solari. On the prediction of settling velocity for plastic particles of different shapes. *Environmental Pollution*, 290:118068, 2021.

K. D. Goral, H. G. Guler, B. E. Larsen, S. Carstensen, E. D. Christensen, N. B. Kerpen, T. Schlurmann, and D. R. Fuhrman. Shields diagram and the incipient motion of microplastic particles. *Environmental Science & Technology*, 2023.

H. G. Guler, B. E. Larsen, O. Quintana, K. D. Goral, S. Carstensen, E. D. Christensen, N. B. Kerpen, T. Schlurmann, and D. R. Fuhrman. Experimental study of non-buoyant microplastic transport beneath breaking irregular waves on a live sediment bed. *Marine Pollution Bulletin*, 181:113902, 2022.

S. A. Hughes. Physical models and laboratory techniques in coastal engineering. *Ocean Engineering*, 7, 1994.

C. Iuppa, G. Passalacqua, and C. Faraci. An equilibrium criterion for plastic debris fate in wave-driven transport. *Marine Pollution Bulletin*, 206:116758, 2024. ISSN 0025-326X. doi: https://doi.org/10.1016/j.marpolbul.2024.116758. URL https://www.sciencedirect.com/science/article/pii/S0025326X24007355.

J. A. Ivar do Sul and M. F. Costa. The present and future of microplastic pollution in the marine environment. *Environmental Pollution*, 185:352–364, 2014. ISSN 0269-7491. doi: https://doi.org/10.1016/j.envpol.2013.10.036. URL https://www.sciencedirect.com/science/article/pii/S0269749113005642.

I. G. Jonsson. Wave boundary layers and friction factors. pages 127–148, 1967.

P. D. Komar and M. C. Miller. Sediment threshold under oscillatory waves. *Coastal Engineering, 756-775.*, 1975.

O. S. Madsen and W. D. Grant. Quantitative description of sediment transport by waves. In *Coastal Engineering 1976*, pages 1092–1112. 1976.

M. Manohar and U. S. B. E. Board. *Mechanics of Bottom Sediment Movement Due to Wave Action*. IER reports. U.S. Beach Erosion Board, 1955. URL https://books.google.it/books?id=mI5uU0sR-ysC.

T. Moeslund. *Introduction to video and image processing: Building real systems and applications*. Undergraduate Topics in Computer Science. Springer, Germany, 2012. ISBN 978-1-4471-2502-0. doi: 10.1007/978-1-4471-2503-7.

P. Nielsen. Three simple models of wave sediment transport. *Coastal Engineering*, 12(1):43–62, 1988.

G. Passalacqua, C. Iuppa, and C. Faraci. A simplified experimental method to estimate the transport of non-buoyant plastic particles due to waves by 2d image processing. *Journal of Marine Science and Engineering*, 11(8), 2023. ISSN 2077-1312. URL https://www.mdpi.com/2077-1312/11/8/1599.

A. Shields. Anwendung der aehnlichkeitsmechanik und der turbulenzforschung auf die geschiebebewegung. *PhD Thesis Technical University Berlin*, 1936.

T. Sui, L. H. Staunstrup, S. Carstensen, and D. R. Fuhrman. Span shoulder migration in three-dimensional current-induced scour beneath submerged pipelines. *Coastal Engineering*, 164:103776, 2021.

L. C. Van Rijn. Unified view of sediment transport by currents and waves. i: Initiation of motion, bed roughness, and bed-load transport. *Journal of Hydraulic engineering*, 133(6):649–667, 2007.

K. Waldschlager and H. Schuuttrumpf. Erosion behavior of different microplastic particles in comparison to natural sediments. *Environmental science & technology*, 53(22):13219–13227, 2019.

H. Zhang. Transport of microplastics in coastal seas. *Estuarine, Coastal and Shelf Science*, 199:74–86, 2017. ISSN 0272-7714. doi: https://doi.org/10.1016/j.ecss.2017.09.032. URL https://www.sciencedirect.com/science/article/pii/S0272771417307254.